Yuan *et al. Chem Synth* 2023;4:31
DOI: 10.20517/cs.2023.19

Chemical Synthesis

Research Article

Open Access

Check for updates

Effect of crystal size of ZSM-11 zeolite on the catalytic performance and reaction route in methanol to olefins

Kai Yuan[1,2,#], Xiang-Yu Jia[1,2,#], Sen Wang[1,*], Sheng Fan[1,2], Shi-Pei He[1,2], Peng-Fei Wang[1], Zhang-Feng Qin[1,*], Mei Dong[1], Wei-Bin Fan[1], Jian-Guo Wang[1,2,*]

[1]State Key Laboratory of Coal Conversion, Institute of Coal Chemistry, Chinese Academy of Sciences, P. O. Box 165, Taiyuan 030001, Shanxi, China.
[2]University of Chinese Academy of Sciences, Beijing 100049, China.
[#]These authors contributed equally to this work.

[*]**Correspondence to:** Prof. Sen Wang, State Key Laboratory of Coal Conversion, Institute of Coal Chemistry, Chinese Academy of Sciences, P. O. Box 165, Taiyuan 030001, Shanxi, China. E-mail: wangsen@sxicc.ac.cn; Prof. Zhangfeng Qin, State Key Laboratory of Coal Conversion, Institute of Coal Chemistry, Chinese Academy of Sciences, P. O. Box 165, Taiyuan 030001, Shanxi, China. E-mail: qzhf@sxicc.ac.cn; Prof. Jianguo Wang, State Key Laboratory of Coal Conversion, Institute of Coal Chemistry, Chinese Academy of Sciences, P. O. Box 165, Taiyuan 030001, Shanxi, China. E-mail: iccjgw@sxicc.ac.cn

How to cite this article: Yuan K, Jia XY, Wang S, Fan S, He SP, Wang PF, Qin ZF, Dong M, Fan WB, Wang JG. Effect of crystal size of ZSM-11 zeolite on the catalytic performance and reaction route in methanol to olefins. *Chem Synth* 2023;4:31. https://dx.doi.org/10.20517/cs.2023.19

Received: 4 Apr 2023 **First Decision**: 5 May 2023 **Revised**: 10 May 2023 **Accepted**: 2 Jun 2023 **Published:** 16 Jun 2023

Academic Editors: Bao-Lian Su, Da-Gang Yu **Copy Editor:** Dan Zhang **Production Editor:** Dan Zhang

Abstract

ZSM-11 zeolite is a promising catalyst for methanol to olefins (MTO); however, its low catalytic stability limits its realistic application. Herein, various ZSM-11 zeolites with different particle sizes were synthesized. The particle size of ZSM-11 has a significant influence on the formation and evolution of reaction intermediates, thereby determining its catalytic performance in MTO. Notably, S-ZSM-11, with a smaller particle size (approximately 400 nm), showed remarkable propene selectivity and catalytic lifetime as high as 42.6% and 243 h, respectively. These values were significantly higher than those observed with larger particle sizes (> 1 μm). The results obtained from gas chromatograph (GC)-MS, ^{13}C MAS NMR, and various isotope-labeling experiments indicated that reduction of crystal size, accompanied by the generation of more intracrystalline mesopores, inhibits the aromatic intermediates formation and decreases the aromatic-based cycle contribution. In contrast, the alkene-based cycle is relatively enhanced, resulting in higher yields of propene and C_{3+} alkenes. Moreover, ethene is mainly produced via the paring route due to the limitation of alkyl side-chain growth of methylbenzenes.Highlights: various ZSM-11 zeolites with different particle sizes were synthesized by the hydrothermal method. S-ZSM-11, with a particle size

of approximately 400 nm, shows superior catalytic performance in methanol to olefins. The propene selectivity and catalytic lifetime reach as high as 42.6% and 243 h, respectively. Decrease of crystal size inhibits the formation of aromatic species and decreases the aromatic-based cycle contribution. Ethene is mainly produced via the paring route.

Keywords: Methanol conversion, light olefins, ZSM-11, particle size, isotope-labeling experiment, reaction route

INTRODUCTION

Conversion of methanol to light olefins (MTO) is an important nonpetroleum route to produce light olefins, as methanol can be easily produced from abundant carbon resources, such as coal, natural gas, and biomass[1,2,3]. The MTO process has been studied for nearly five decades, and it has been widely acknowledged that the formation of light olefins is simultaneously controlled by the hydrocarbon pool (HCP) mechanism, including the alkene-based cycle and arene-based cycle[4-8]. The alkene-based cycle mainly produces propene and long-chain olefins (C_{3+} alkenes) through successive methylations and cracking or elimination reaction, whereas ethene and part of propene are mainly obtained by the arene (or aromatic)-based cycle with polymethylbenzenes (polyMBs) as the dominant HCP species[4,9]. This indicates that enhancing the contribution of an alkene-based cycle can significantly promote the formation of propene. An efficient method to achieve this is by decreasing the acidic content and strength of zeolite and regulating the distribution of acid sites. These measures can weaken the hydrogen transfer and aromatization reactions, thereby inhibiting the generation of aromatic intermediates and lowering the contribution of the aromatic-based cycle[10,11]. According to the detailed formation pathway, the aromatic-based cycle can be divided into a side-chain route and a paring route, in which the paring route involves the benzene ring contraction/expansion that incorporates the carbon atoms of the aromatic ring into olefin products, while only the alkyl side-chain of aromatics is directly linked to the formed olefins in the side-chain route[12-18].

Acidic zeolite, with its unique pore structure, tunable acidic properties, and high thermal/hydrothermal stability, is considered to be the most important catalyst in MTO. Although SAPO-34 and ZSM-5 zeolites have been widely used in industry[19-22], they still have the problems of poor catalytic stability or low target product selectivity, indicating that the development of high-performance MTO catalysts is not outdated. Recently, ZSM-11 (MEL) zeolite has attracted much attention in MTO due to its specific channel structure. This zeolite has two straight channels with a pore size of 5.3 × 5.4 Å that interacted, forming two intersectional cavities (9 Å and 11.7 Å). The crystalline features and the size of the pore channel of ZSM-11 are similar to those of ZSM-5, which possesses one straight channel (5.3 Å × 5.6 Å) and one sinusoidal channel (5.1 Å × 5.5 Å)[23]. However, some recent investigations indicate that ZSM-11 zeolite [especially the sample with a high Si/Al ratio (> 100)] exhibits significantly lower catalytic stability than ZSM-5[24-26], which limits its realistic application in MTO. Consequently, improving the performance of ZSM-11 zeolite in MTO, especially the catalytic lifetime, has become the focus of research.

In our previous works, we found that the catalytic activity and product selectivity of ZSM-11 in MTO can be regulated by tuning acid site distribution in the framework through introducing proper content of boron (B)[24,27], alkali metal ions[28], or halogen anions[29] in the synthesis gel. Nevertheless, the long-term stability of the ZSM-11 sample with a high Si/Al ratio is still not satisfactory. Another more effective way to increase lifetime is to reduce particle size or introduce more mesoporous. Shen *et al.* demonstrated that more coke species are generated in MTO over zeolite with larger crystal sizes[23]. This is because a longer diffusion path provides sufficient residence time for aromatic species to react with Brønsted acid sites (BAS), leading to

serious carbon deposition. Similar phenomenons were also observed over Beta[30], SAPO-34[31], SSZ-13[32], ZSM-22[33], and ZSM-58[34] zeolites. These results indicate that regulation of the particle size will be a simple but effective method to improve the catalytic stability of ZSM-11; however, relevant studies are rarely reported. Moreover, the effect of particle size on the formation and structural evolution of active intermediates and the catalytic pathway remains unclear, which also limits the development of high-performance ZSM-11 zeolite catalysts.

In this work, various ZSM-11 zeolites with different particle sizes but highly comparable crystallinity, chemical composition, and acidic properties were synthesized. The catalytic performance and reaction route of these samples in MTO were thoroughly investigated by GC-MS, ^{13}C MAS NMR, transient $^{12}C/^{13}C$ methanol switching experiment, and a co-feeding experiment involving ^{13}C-methanol with ^{12}C-propene, ^{12}C-n-butene, or ^{12}C-benzene.

EXPERIMENTAL

ZSM-11 zeolites preparation

ZSM-11 zeolites with different particle sizes were synthesized by the hydrothermal method by changing the water content during synthesis. Silica sol (JN-40), sodium aluminate ($NaAlO_2$), and sodium hydroxide (NaOH) were used as a silicon source, aluminum source, and alkaline source, respectively. Tetrabutylammonium hydroxide (TBAOH) was performed as the organic template. During synthesis, 39.52 g or 19.36 g of H_2O, 7.27 g of TBAOH, 0.05 g of $NaAlO_2$, 0.31 g of NaOH, and 9.68 g of JN-40 were added sequentially, and the mixture was then stirred for 24 h at 30 °C. The molar composition of resulted gel mixture was 9 TBAOH: 0.3214 Al_2O_3: 90 SiO_2: n H_2O: 12.897 NaOH (n = 3600 and 2160, respectively). The synthesis gel was sealed into a Teflon-lined stainless steel autoclave and synthesized at 85 °C for 48 h, then at 120 °C for 48 h, and finally at 165 °C for 20 h under rotation of 15 rpm. The prepared samples were labeled as L-ZSM-11 (n = 3600) and M-ZSM-11 (n = 2160), respectively.

To further reduce the crystal size, nanosized ZSM-11 zeolite was prepared through a recrystallization method. First, the parent ZSM-11 zeolite was synthesized with the molar composition of 9 TBAOH: 0.225 Al_2O_3: 90 SiO_2: 1065 H_2O: 12.897 NaOH, following the same crystallization procedure as described above. Afterward, 1 g of calcined parent zeolite was suspended in 10 mL TBAOH solution (0.7 M) and then heated at 165 °C for 72 h under static conditions. The obtained sample was defined as S-ZSM-11.

The as-synthesized Na-type ZSM-11 was transformed into the H-type ZSM-11 through ion exchange with NH_4NO_3 solution. The resulting sample was then dried at 120 °C overnight and calcinated at 560 °C for 10 h.

Catalyst characterization

The framework topological structure of zeolites was identified by X-ray diffraction (XRD) measured on a Rigaku MiniFlex II desktop X-ray diffractometer at 30 kV, 15 mA using Cu Kα radiation. The average particle size and morphology of zeolites were characterized by field emission scanning electron microscopy (FE-SEM) images (JEOL JSM-7001F, Japan). The transmission electron microscopy (TEM) images of samples were measured on a field emission transmission electron microscope using JEM 2100-F, JEOL, Japan.

The textural properties were evaluated by N_2 sorption on a Micrometritics TriStar II 3020 analyzer. Before testing at-196 °C, the catalysts were first degassed at 300 °C under high vacuum for 10 h. The surface area and micropore volume were obtained using the Brunauer-Emmett-Teller (BET) and the t-Plot method,

respectively. The isotherms of *o*-xylene vapor adsorption were collected on a BELSORP-max high-precision adsorption analyzer at room temperature. The sample pretreatment program was the same as that of N_2 sorption.

Inductively coupled plasma optical emission spectrometry (ICP-OES, icap6300) was performed to determine the Si/Al ratio of zeolites. NH_3 temperature-programmed desorption (NH_3-TPD) was conducted on a Micrometritics AutoChem II 2920 analyzer. A U-type quartz tube was loaded with 100 mg of catalyst and pretreated at 550 °C under He flow (30 mL/min) for 2 h. After that, the sample was cooled to 120 °C and allowed to saturated adsorption for NH_3. After thorough flushing with He, the NH_3-TPD profile was recorded by increasing the temperature from 120 to 550 °C at a rate of 10 °C min^{-1}. The thermal conductivity detector (TCD) was employed to monitor the desorbed NH_3.

The pyridine adsorption infrared spectra (Py-IR, Bruker Tensor 27) were used to evaluate the Brønsted and Lewis acid content of zeolites. First, the zeolite thin wafer was pretreated for 2 h at 400 °C under 10^{-2} Pa. Then, it was cooled to 35 °C to allow saturated adsorption of pyridine vapor for 30 min. Subsequently, physical-adsorbed pyridine was removed at 150 °C. The concentrations of BAS and Lewis acid sites (LAS) (C, μmol g^{-1}) were calculated using the following equation by integrating the area of peaks at 1540 and 1450 cm^{-1}, respectively[35]:

$$C = (A/\varepsilon) \times (S/m) \times 1000$$

where A is the area of peak at 1540 or 1450 cm^{-1}, S is the wafer surface area (1.33 cm^2), ε is the molar extinction coefficient (1.13 and 1.28 cm μmol^{-1} for BAS and LAS, respectively), and m is the mass of sample (mg). The amounts of BAS on the external surface of ZSM-11 were determined from the FT-IR spectra of 2,6-ditert-butylpyridine (dTBPy) adsorption at 150 °C[36,37]. The detailed experimental procedure is similar to that of Py-IR.

The thermogravimetric analysis (TGA) carried out on a Rigaku Thermo Plus Evo TG 8120 thermogravimetric analyzer was used to evaluate the content of deposited coke species. In this analysis, 10 mg of the spent catalyst was heated under air flow from 30 to 800 °C at a rate of 5 °C min^{-1}.

The ^{27}Al and ^{13}C solid-state magic angle spinning (MAS) NMR spectra were performed on a 600 MHz Bruker Avance spectrometer (magnetic field of 14.1 T). The chemical shift for ^{27}Al MAS NMR and ^{13}C MAS NMR spectra were referenced to 1 M $Al(NO_3)_3$ solution and hexa-methylbenzene(MB), respectively[38]. The deconvolution of ^{27}Al MAS NMR ranging from 45 to 65 ppm was conducted using the Gauss-Lorentz equation[24,28].

Catalytic evaluation

The methanol conversion experiment was conducted at 450 °C and 1 atm in a fixed-bed reactor made of stainless steel, as depicted in Supplementary Figure 1. Prior to the experiment, 500 mg of catalyst (20-40 mesh) was first pretreated under N_2 flow at 550 °C for 4 h. Methanol was then pumped into the reactor using an infusion pump, with N_2 (40 mL min^{-1}) serving as the diluting gas. The methanol weight-hourly space velocity (WHSV) was set at 3.8 h^{-1}. The Agilent 7890A GC equipped with one TCD and two flame ionization detectors (FID) detectors was used for online analysis of the gaseous products. Another two Agilent 7890A GCs (involving one FID and one TCD) were used for offline analysis of liquid and oil products. The conversion of methanol (x) and the selectivity of various products (s_i) were calculated by the equations:

$$X = (n_{methanol,in}\text{-}n_{methanol,out})/n_{methanol,in} \times 100\%$$

$$s_i = n_i k_i / \sum n_i k_i \times 100\%$$

where n_i and k_i are the molar number and carbon atom number of product i in the effluents, respectively. Dimethyl ether (DME) is regarded as unconverted methanol during the reaction.

Isotopic labeling experiments

Transient $^{12}C/^{13}C$ methanol switching experiment

The transient $^{12}C/^{13}C$ methanol switch experiments were conducted in a pulse reactor, as described in Ref[39]. The ^{12}C-methanol was first introduced into the reactor under Ar (22 mL min^{-1}) flow using a methanol saturator (kept at 0 °C). After a reaction time of 30 min, the ^{12}C-methanol feed was stopped, and three ^{13}C methanol pulses were successively introduced into the reactor.

Co-feeding of ^{13}C-methanol and ^{12}C-propene or ^{12}C-butene

The n-propanol and n-butanol were used as the precursor of propene and butene, as they could be instantaneously dehydrated to propene and butene on acidic zeolite[6,40]. The ^{13}C-methanol and ^{12}C-n-propanol were simultaneously fed into the reactor by flowing Ar through the methanol and propanol saturators, which were kept at 0 °C and 28 °C, respectively. This results in the partial pressures of methanol and n-propanol being 3.9 and 3.3 kPa, respectively. The flow of Ar carrier gas was 24 mL/min for methanol and 5.3 mL/min for n-propanol to make the methanol:n-propanol molar ratios of 5.4.

For the co-feeding of ^{13}C-methanol and ^{12}C-n-butanol, the methanol and ^{12}C-n-butanol saturators were kept at 0 °C and 28 °C, respectively. This results in the partial pressures of methanol and n-butanol being 3.9 and 1.1 kPa, respectively. The flow of Ar carrier gas was 24 mL/min for methanol and 16.4 mL/min for n-butanol to make the methanol:n-butanol molar ratios of 5.4.

Co-feeding of ^{13}C-methanol and ^{12}C-benzene

The procedure for the co-feeding experiment involving ^{13}C-methanol and ^{12}C-benzene is similar to that of co-feeding of ^{13}C-methanol and ^{12}C-propene or ^{12}C-butene, except that the ^{13}C-methanol and ^{12}C-benzene saturators were kept at 28 °C, and corresponding partial pressures of methanol and benzene were 19.7 and 14.5 kPa, respectively. The flow of Ar carrier gas was 24 mL/min for methanol and 6 or 3 mL/min for benzene to make the methanol:benzene molar ratios of 5.4 or 10.8.

Analyses of the effluents and retained species in zeolite catalyst

The gaseous products in the effluents and the retained species on catalysts were analyzed by Shimadzu QP2010 GC-MS. The detailed method for calculating the isotopic distribution can refer to the work of Price *et al*[41].

RESULTS AND DISCUSSION

Crystal structure and texture property of various ZSM-11 zeolites

Figure 1A displays the XRD patterns of various prepared ZSM-11 zeolites. It is found that all samples exhibit a pure MEL phase, with typical characteristic peaks at 2θ of 7.92°, 8.78°, 23.14°, and 23.98°. The morphology and particle size of these ZSM-11 zeolites are evaluated by SEM and TEM images [Figure 1D-I]. These three samples have spherical structures, with the average particle size decreasing in the order of L-ZSM-11 (2.2 μm) > M-ZSM-11 (0.8 μm) > S-ZSM-11 (0.4 μm). Moreover, abundant intracrystalline mesopores are observed on S-ZSM-11 due to the aggregation of small nanosized spherical-like crystals [Figure 1I].

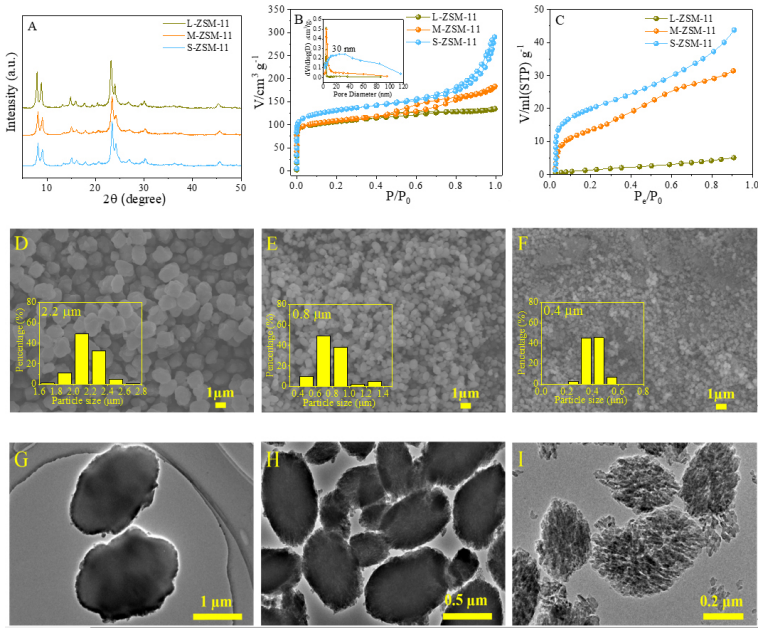

Figure 1. XRD patterns (A); N_2 adsorption-desorption isotherms and pore size distribution curves (B); *o*-xylene vapor adsorption isotherms (C); and SEM images (D-F) (insert: particle size distribution) and TEM images (G-I) of L-ZSM-11 (D, G); M-ZSM-11 (E, H); and S-ZSM-11 (F, I) zeolites.

According to the results of N_2 adsorption-desorption isotherms, an obvious hysteresis loop in the region of $0.7 < P/P_0 < 1.0$, corresponding to the capillary condensation in the intracrystal mesopores, is verified in S-ZSM-11, while it gradually attenuates in M-ZSM-11 and L-ZSM-11 [Figure 1B]. The curves of pore size distributions further confirm the existence of mesopores (c.a. 30 nm) in S-ZSM-11. As a result, S-ZSM-11 exhibits a larger external surface area (155 $m^2 g^{-1}$) and mesoporous volume (0.31 $cm^3 g^{-1}$) than those of M-ZSM-11 (102 $m^2 g^{-1}$ and 0.17 $cm^3 g^{-1}$) and L-ZSM-11 (87 $m^2 g^{-1}$ and 0.10 $cm^3 g^{-1}$), despite that they have similar micropore surface area and micropore volume [Table 1]. The *o*-xylene vapor adsorption isotherms give additional evidence that the uptake rate and adsorption capacity of *o*-xylene are considerably increased over S-ZSM-11 due to its smaller crystallite size and greater presence of intracrystalline mesopores [Figure 1C].

Elemental composition, distribution, and acidity of various ZSM-11 zeolites

All the prepared ZSM-11 zeolites exhibit a similar Si/Al molar ratio, as indicated by ICP-OES

Meanwhile, most aluminum species are incorporated into the zeolite framework, as observed by an intense peak at around 45-65 ppm, but a very weak one at ~0 ppm in ^{27}Al MAS NMR, which are corresponded to the framework aluminum and extra-framework aluminum, respectively [Supplementary Figure 2]. Deconvolution of ^{27}Al MAS NMR indicates that the peaks at 48.5, 55.6, and 58.1 ppm can be assigned to the aluminum atoms in the T3, T4 + T6, and T5 lattice sites of the intersection cavity, while that at 53.2 ppm is resulted from the siting of aluminum atoms in the T1 + T2 + T7 lattice sites of the straight channel [Figure 2A][24,28,30,42,43]. It can be found that no evident variation in Al atoms distribution is observed over L-ZSM-11, M-ZSM-11, and S-ZSM-11 [Supplementary Table 1].

The acidic properties of ZSM-11 samples were analyzed by NH_3-TPD, Py-IR, and dTBPy-IR, as depicted in Figure 2B, C, and D. In the NH_3-TPD profiles, the peaks at around 175 °C and 350°C are ascribed to the interaction of ammonia molecule with weak acid and strong acid sites, respectively. It can be found that all

Table 1. Relative crystallinity and textural properties of various ZSM-11 zeolites

Zeolite	Crystal size (μm)	Crystallinity (%)	Surface area ($m^2 g^{-1}$)			Pore volume ($cm^3 g^{-1}$)		
			total	micro	ext	total	micro	meso
L-ZSM-11	2.2	100	335	248	87	0.21	0.11	0.10
M-ZSM-11	0.8	94	343	241	102	0.28	0.11	0.17
S-ZSM-11	0.4	98	416	261	155	0.43	0.12	0.31

The average crystal size was estimated by counting about 200 zeolite crystal particles in the SEM image. The relative crystallinity of various ZSM-11 zeolites was obtained by comparing their peak intensity for the (5 0 2) and (3 0 3) facets at 23.0° and 23.8° in the XRD patterns to that of L-ZSM-11. The surface area and pore volume were determined on the basis of nitrogen physisorption data by using the BET method and t-Plot method, respectively.

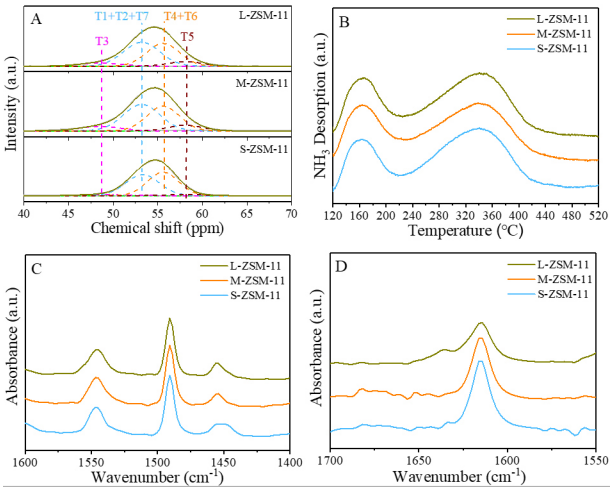

Figure 2. Deconvoluted ^{27}Al MAS NMR spectra (A); NH_3-TPD profiles (B); Py-IR spectra (C); and dTBPy-IR spectra (D) of L-ZSM-11, M-ZSM-11, and S-ZSM-11 zeolites.

samples have similar acid content and acid strength [Figure 2B and Table 2][44]. This is similar to the result of Py-IR. The peaks at 1540 and 1450 cm^{-1} are assigned to the desorption of pyridine from BAS and LAS, respectively. As expected, the difference in Brønsted acid and Lewis acid content of L-ZSM-11, M-ZSM-11, and S-ZSM-11 is not significant [Figure 2C and Table 2]. In addition, the results of dTBPy-IR indicate that all three samples have comparable external Brønsted acid content [Figure 2D and Table 2].

Catalytic results of various ZSM-11 zeolites in MTO

The catalytic performance of various ZSM-11 zeolites in methanol conversion was evaluated [Figure 3A-C and Supplementary Table 2]. A much higher catalytic lifetime and larger turnover numbers (TONs) are observed on S-ZSM-11 (243 h and 3.5×10^5) than on M-ZSM-11 (134 h and 1.9×10^5) and L-ZSM-11 (74 h and 1.1×10^5). As expected, S-ZSM-11 has the lowest coking rate, with the slowest rate of micropore surface area and micropore volume reduction [Figure 3D-F]. Besides the catalytic stability, L-ZSM-11, M-ZSM-11, and S-ZSM-11 are also different in the product distribution. S-ZSM-11 exhibits higher selectivity to propene (42.6%) and long-chain alkenes ($C_4^=$ + $C_5^=$) (39.2%), but lower to ethene (4.9%), aromatics (2.7%), and C_1-C_5 alkanes (6.5%), in comparison with L-ZSM-11 (39.2% to propene, 36.6% to long-chain alkenes ($C_4^=$ + $C_5^=$), 7.8% to ethene, 7.6% to C_1-C_5 alkanes, and 5.1% to aromatics), while the product selectivities of M-ZSM-11 are in the middle of S-ZSM-11 and L-ZSM-11. Moreover, S-ZSM-11 gives higher values of 2-MB/E (1.6) and (P–E)/E (7.7) than those of M-ZSM-11 (1.3 and 6.5) and L-ZSM-11 (0.8 and 4.1), indicating that the alkene-based cycle is more significant in methanol conversion on the S-ZSM-11 than on the other two zeolites.

Table 2. Elemental composition and acidic properties of various ZSM-11 zeolites

Zeolites	Si/Al by ICP	Acidity by NH_3-TPD (μmol g^{-1})			Acidity by Py-IR or dTBPy-IR (μmol g^{-1})			
		weak	strong	total	Brønsted	Lewis	total	external Brønsted
L-ZSM-11	101	49	115	164	86	27	113	19
M-ZSM-11	105	51	107	158	83	26	109	25
S-ZSM-11	111	45	117	162	84	34	118	28

The Si/Al ratio was measured by ICP-OES; The quantities of weak and strong acid sites were determined by NH_3-TPD. The quantities of Brønsted and Lewis acid sites were acquired by Py-IR, according to the amounts of pyridine (Py) desorbed at 150 °C. The quantities of external Brønsted acid were tested by dTBPy-IR, according to the amounts of dTBPy desorbed at 150 °C.

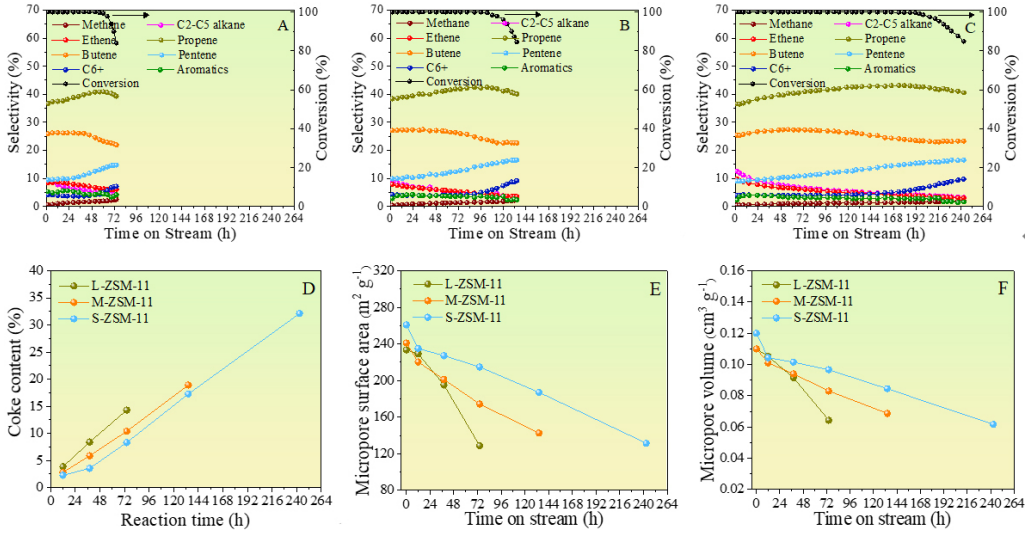

Figure 3. Methanol conversion and product selectivity with the time on stream for MTO over L-ZSM-11 (A); M-ZSM-11 (B); and S-ZSM-11 (C) zeolites; the coke content (D); micropore surface area (E); and micropore volume (F) as a function of time on stream in MTO over these three samples. The reactions were performed at 0.1 MPa, 450 °C, and methanol WHSV of 3.8 h^{-1}.

To better eliminate the effects of secondary reactions, the catalytic test for MTO was also carried out at sub-complete conversion of methanol (approximately 18%), and the results were given in Figure 4A and Supplementary Table 3. Even under these conditions, S-ZSM-11 maintains higher selectivity toward propene (41.2%) and C_4-C_6 aliphatics (51.6%) while exhibiting lower selectivity toward ethene (4.8%) and aromatics (0.7%) compared to those of M-ZSM-11 (8.2% to ethene, 2% to aromatics, 39.7% to propene, and 47.9% to C_4-C_6 aliphatics) and L-ZSM-11 (11.6% to ethene, 3.7 % to aromatics, 37.4% to propene, and 45.3% to C_4-C_6 aliphatics). Meanwhile, S-ZSM-11 also demonstrates higher values of 2MB/E and (P–E)/E (2.5 and 7.6, respectively) in comparison to M-ZSM-11 (1.3 and 3.8) and L-ZSM-11 (0.9 and 2.2). Therefore, the variation in product distribution confirms that decrease of the particle size of ZSM-11 zeolite can significantly enhance the alkene-based cycle in MTO[30,45].

Another point should be noticed that different methanol weight hours space velocity ($WHSV_{methanol}$) was used for MTO over these three samples to achieve the iso-conversion of methanol. Considering the $WHSV_{methanol}$ of L-ZSM-11(19.0 h^{-1}) is much higher than that of M-ZSM-11 (9.5 h^{-1}) and S-ZSM-11(8.7 h^{-1}), L-ZSM-11 should have higher initial activity for methanol conversion than the other two samples. This is verified by performing MTO reaction at the same $WHSV_{methanol}$ (9.5 h^{-1}). As shown in Figure 4B, the

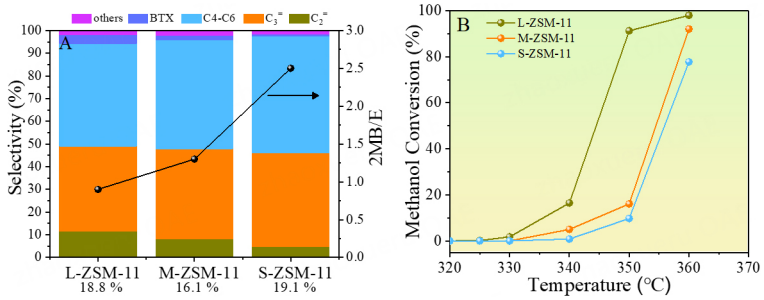

Figure 4. (A) Product selectivity and 2-MB/E ratio over various ZSM-11 zeolites under iso-conversion of methanol (about 18 %) at 350 °C and 30 min time on stream; (B) Variation of methanol conversion rate with the reaction temperature over various ZSM-11 zeolites at the same $WHSV_{methanol}$.

methanol conversion rate is faster on L-ZSM-11 than on M-ZSM-11 and S-ZSM-11. One possible reason is that smaller particle sizes and the higher presence of intracrystalline mesopores of S-ZSM-11 shorten the diffusion path and decrease the interaction of methanol with BAS, thereby producing fewer active HCP intermediates during the initial methanol conversion process.

Influence of crystal size of ZSM-11 on the formation and evolution of initial HCP species in MTO

To evaluate the effect of the crystal size of ZSM-11 on the type and structure of initial HCP species, GC-MS, ^{13}C MAS NMR, and $^{12}C/^{13}C$ methanol switching experiments were carried out.

After continuous flowing of $^{13}CH_3OH$ at 350 °C for varying reaction times, the catalyst was cooled by liquid nitrogen and then measured by ^{13}C MAS NMR. As shown in Figure 5A and 5B, the strong signal peaks at 50 and 59.5 ppm represent the physisorbed methanol and DME[46], while peaks at 10-30 ppm and around 130 ppm are assigned to the carbon atoms of methyl group and benzene ring of polyMBs, respectively[47,48]. Regardless of the reaction time, L-ZSM-11 gives a stronger intensity of peaks characteristic of polyMBs than that of M-ZSM-11 and S-ZSM-11.

This result is further supported by the GC-MS analysis. After reaction for 1 min at 300 °C, certain amounts of polyMBs are detected on GC-MS, and their content is gradually increased in the order of S-ZSM-11 < M-ZSM-11 < L-ZSM-11 [Figure 5C]. Notably, higher polyMBs (e.g. tetra-, penta-, and hexa-MBs) accounts for 56% of the total carbonaceous species over L-ZSM-11, followed by M-ZSM-11 (43%) and S-ZSM-11 (28%). Such a phenomenon becomes more evident when the reaction is conducted at 350 °C for 1 min [Figure 5D]; a significantly higher amount of polyMBs is observed on L-ZSM-11 than on M-ZSM-11 and S-ZSM-11. Undoubtedly, increase of the crystal size of ZSM-11 zeolite promotes the formation and growth of aromatic-based intermediates (e.g., polyMBs). However, S-ZSM-11, with a smaller particle size and greater intracrystalline mesoporosity, shows the lowest rate of polyMB formation, thus weakening the methanol initial conversion capacity and prolonging the reaction induction period, as observed in Figure 4B.

The reactivity of polyMBs in MTO was further evaluated by a $^{12}C/^{13}C$ methanol switching experiment over L-ZSM-11 and S-ZSM-11. After $^{12}CH_3OH$ conversion at 350 °C for 30 min, the ^{12}C-methanol was stopped, and three ^{13}C-methanol pulses were then successively injected with an interval of 3 min. As shown in Figure 5E and 5F, L-ZSM-11 exhibits higher total ^{13}C-labeled content of tetra-, penta-, and hexa-MBs, but lower to xylene and triMBs, in comparison with those of S-ZSM-11. This gives another piece of evidence that decrease of the crystal size of ZSM-11 inhibits the formation of higher polyMBs, in good agreement with the observation of ^{13}C MAS NMR and GC-MS.

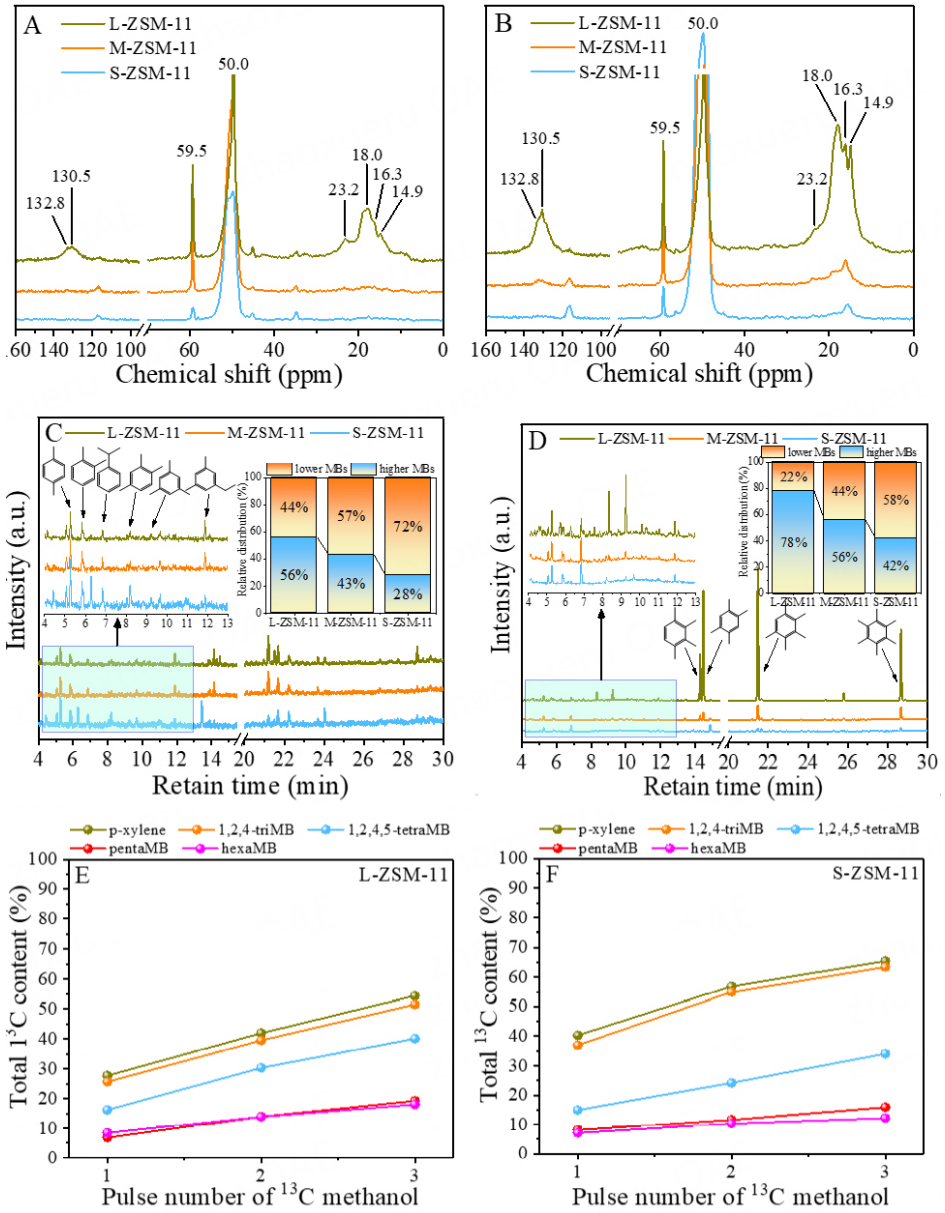

Figure 5. ^{13}C MAS NMR spectrum of the retained organic intermediates in three ZSM-11 zeolites after continuous flow $^{13}CH_3OH$ reaction at 350 °C for 1 min (A) and 30 min (B); respectively. GC-MS chromatograms of retained organic species obtained from the reaction of ^{13}C methanol for 1 min at 300 °C (C) and 350 °C (D); respectively; the inserted histogram represents the relative proportion of higher and lower polyMBs estimated from corresponding GC-MS chromatograms. Total ^{13}C-labeled content (%) in the retained aromatics (xylene to hexaMB) for MTO over L-ZSM-11 (E) and S-ZSM-11 (F) at 350 °C.

Influence of crystal size of ZSM-11 on the dual cycle mechanism

Co-feeding of ^{13}C-methanol and ^{12}C-propene or n-butene

The influence of the crystal size of ZSM-11 on the aromatic-based cycle and alkene-based cycle was investigated through the co-feeding of ^{13}C-labeled methanol with ^{12}C-propene or ^{12}C-butene. After reaction at 350 °C for 120 s, the total ^{13}C-labeled content and the isotopomer distributions of light olefins and polyMBs are depicted in Figures 6 and 7. For co-feeding ^{13}C-methanol and ^{12}C-propene, the total ^{13}C-labeled content of ethene and polyMBs is about 12.5% and 4.8–13.5% higher on L-ZSM-11 than on S-ZSM-11, whereas the difference in the total ^{13}C-labeled content of C_{3+} olefins is below 3% over these two samples.

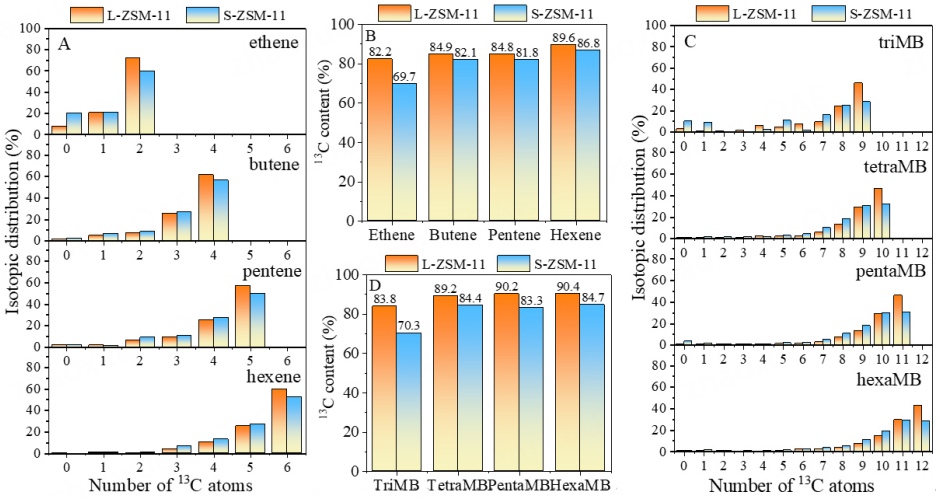

Figure 6. The total ^{13}C content and isotopic labeling patterns in the effluent olefins (A, B) and retained polyMBs (C, D) after co-reacting ^{13}C-methanol with ^{12}C-propene (molar ratio 5.4:1) for 120 s over L-ZSM-11 and S-ZSM-11 at 350 °C.

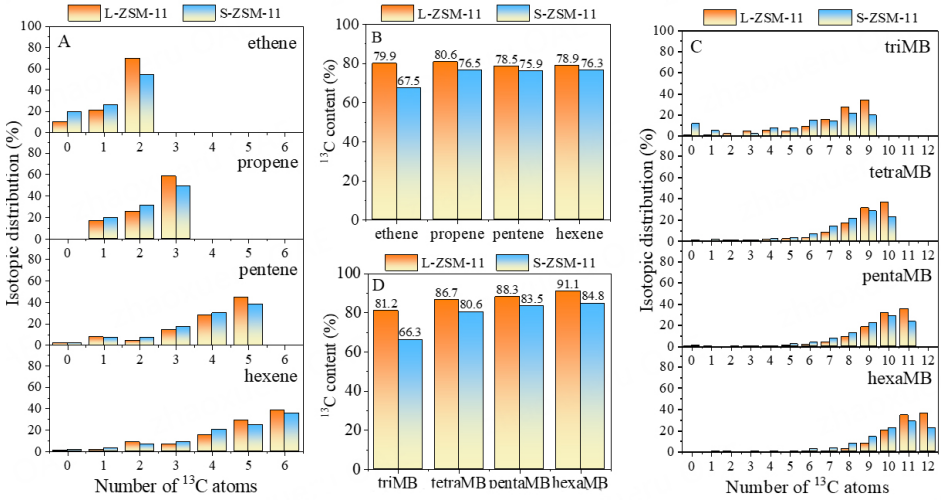

Figure 7. The total ^{13}C content and isotopic labeling patterns in the effluent olefins (A, B) and retained polyMBs (C, D) after co-reacting ^{13}C-methanol with ^{12}C-n-butene (molar ratio 5.4:1) for 120 s over L-ZSM-11 and S-ZSM-11 at 350 °C.

When the ^{12}C-propene is replaced by ^{12}C-n-butene, a similar result is observed; L-ZSM-11 shows higher total ^{13}C-labeled content of ethene (79.9%) and polyMBs (81.2-91.1%) than that of S-ZSM-11 (67.5% for ethene and 66.3–84.8% for polyMBs); however, both of the two samples give highly comparable total ^{13}C-labeled content of C_{3+} olefins. These results indicate that decrease of the crystal size of ZSM-11 zeolite suppresses the aromatic-based cycle, leading to decrease of the generation of ethene and polyMBs.

Co-feeding of ^{13}C-methanol and ^{12}C-benzene

Since the aromatic-based cycle involves both the side-chain route and paring route [Scheme 1], the influence of the crystal size of ZSM-11 on these two routes was analyzed by co-feeding of ^{13}C-methanol with ^{12}C-benzene at 350 °C for different times. According to the isotopomer distributions, ethene containing two ^{13}C atoms ($^{13}CH_2$=$^{13}CH_2$) should be produced through the side-chain route, while ethene with two ^{12}C ($^{12}CH_2$=$^{12}CH_2$) or one ^{12}C and one ^{13}C atom ($^{12}CH_2$=$^{13}CH_2$) is mainly derived from the paring route. This is because

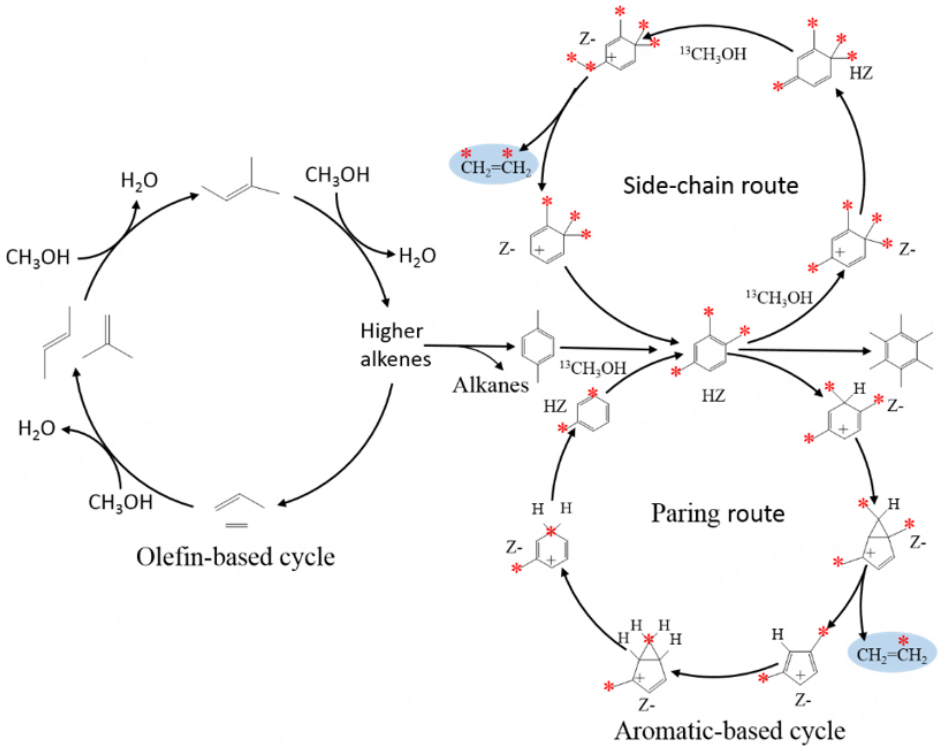

Scheme 1. The proposed dual cycle mechanism for light olefins formation over ZSM-11 zeolite in MTO.

only the paring route, involving the benzene ring contraction/expansion, can incorporate the carbon atoms from the aromatic ring into the olefin product.

As depicted in Figure 8A, with the increase of reaction time from 30 s to 120 s, the proportion of $^{13}CH_2=^{13}CH_2$ gradually elevates from 28% to 52%, while that of $^{12}CH_2=^{12}CH_2$ and $^{12}CH_2=^{13}CH_2$ is decreased over L-ZSM-11, indicating the enhancement of side-chain route. However, for S-ZSM-11 [Figure 8B], even after a reaction time of 120 s, $^{12}CH_2=^{12}CH_2$ and $^{12}CH_2=^{13}CH_2$ still account for 64% of ethene. This suggests that the paring route is dominant in ethene formation over S-ZSM-11. When the molar ratio of ^{13}C-methanol:^{12}C-benzene is increased to 10.8, similar results are obtained; the paring route contributes more to the ethene formation on S-ZSM-11 than on L-ZSM-11 [Supplementary Figure 3]. This phenomenon can be rationalized by that reduction of crystal size, accompanied by the increase in intracrystalline mesoporous structure, which decreases the interaction of methanol with polyMBs intermediates, thereby inhibiting the alkyl side-chain growth. As a result, the side-chain route is relatively inhibited over S-ZSM-11. Notably, according to the isotope distribution of ^{13}C atoms in polyMBs [Figure 8C], the majority of the polyMBs are generated from alkylation of ^{13}C-methanol with ^{12}C-benzene, whereas the contribution from sole ^{13}C methanol is not evident within such short times (≤ 120 s)[9,49].

According to the above results, it can be concluded that reduction of crystal size of ZSM-11 (e.g., S-ZSM-11) and increasing intracrystalline mesoporosity effectively inhibits the aromatic intermediates formation and decreases the aromatic-based cycle contribution. In contrast, the alkene-based cycle is enhanced, resulting in higher yields of propene and C_{4+} alkenes, along with an extended catalytic lifetime. In addition, S-ZSM-11 shows a higher diffusion ability that weakens the interaction of methanol with polyMBs intermediates. As a result, the growth of the alkyl side-chain on the benzene ring is inhibited, leading to a decreased contribution of the side-chain route in methanol conversion. Notably, reduction of the crystal size of ZSM-

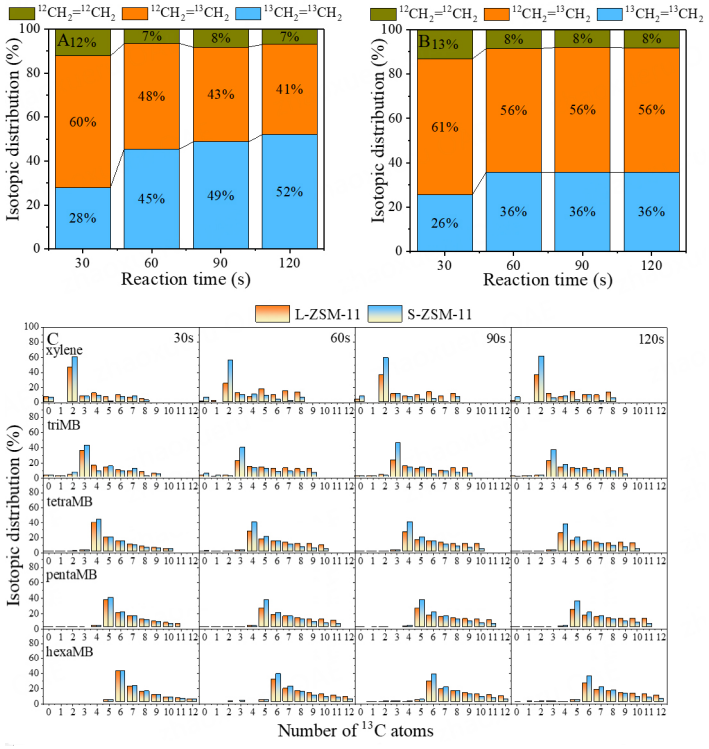

Figure 8. Distribution of ^{13}C atoms in ethene over L-ZSM-11 (A) and S-ZSM-11 (B) and isotopic labeling patterns of retained polyMBs (C) (xylene to hexaMB) after different reaction times of co-reacting ^{13}C-methanol with ^{12}C-benzene (molar ratio 5.4:1) at 350 °C.

11 to below 150 nm may further improve the catalytic lifetime[23]; however, this needs more complex synthesis conditions. In addition, excessively small crystal sizes can make the solid-liquid separation process more challenging. Therefore, considering the synthesis cost and reaction performance, we tentatively suggest that the crystal size in the range of 150-400 nm may be more suitable for the practical application of ZSM-11 zeolite in MTO.

CONCLUSIONS

Various ZSM-11 zeolites with different crystal sizes but highly comparable crystallinity, chemical composition, and acidic properties were prepared. The influence of the crystal size of ZSM-11 on the catalytic performance and reaction route in MTO was systemically investigated by GC-MS, ^{13}C MAS NMR, and various isotope-labeling experiments. The results indicated that S-ZSM-11, with a smaller crystal size and more intracrystalline mesoporosity, exhibited superior catalytic performance in MTO, with the propene selectivity and catalytic lifetime reaching 42.6% and 243 h, respectively. Meanwhile, reduction of crystal size of ZSM-11 considerably inhibited the formation of aromatic intermediates (especially higher polyMBs) and suppressed the aromatic-based cycle. In contrast, the alkene-based cycle was relatively enhanced, which generated more propene and C_{3+} alkenes. Moreover, the co-feeding experiment involving isotope-labeling ^{13}C-methanol and ^{12}C-benzene confirmed that ethene is mainly produced through the paring route, as the alkyl side-chain growth of aromatic intermediates suffers from limitation over S-ZSM-11. This work not only provides an efficient method to significantly improve the catalytic performance of ZSM-11 zeolite in MTO but also unravels the influence of the crystal size of zeolite on the formation and structural evolution of active intermediates and the catalytic route.

DECLARATIONS

Authors' contributions

Writing-original draft, Visualization, Validation, Methodology, Investigation, Data curation:Yuan K
Writing-original draft, Validation, Methodology, Investigation: Jia XY
Writing-review & editing, Visualization, Validation, Supervision, Methodology, Investigation, Data curation, Conceptualization: Wang S
Validation, Methodology, Investigation: Fan S, He SP, Wang PF
Supervision, Methodology, Investigation, Conceptualization: Qin ZF
Validation, Resources, Project administration, Methodology. Funding acquisition: Dong M
Supervision, Resources, Project administration, Investigation, Funding acquisition, Conceptualization: Fan WB
Writing-review & editing, Visualization, Validation, Supervision, Resources, Investigation, Conceptualization: Wang JG

Availability of data and materials

The data that support the findings of this study are available from the corresponding authors upon reasonable request.

Financial support and sponsorship

The authors are grateful to the financial support of the National Key R&D Program of China (2020YFA0210900); the National Natural Science Foundation of China (U1910203; 21991090; 21991092; U22A20431; 22272195); the Natural Science Foundation of Shanxi Province of China (202203021224009); Youth Innovation Promotion Association CAS (2021172); Excellent doctoral student award, and subsidy program of Shanxi Province (BK2018001).

Conflicts of interest

All authors declared that there are no conflicts of interest.

Ethical approval and consent to participate

Not applicable.

Consent for publication

Not applicable.

REFERENCES

1. Chang C. The conversion of methanol and other O-compounds to hydrocarbons over zeolite catalysts. *J Catal* 1977;47:249-59. DOI
2. Olsbye U, Svelle S, Bjørgen M, et al. Conversion of methanol to hydrocarbons: how zeolite cavity and pore size controls product selectivity. *Angew Chem Int Ed Engl* 2012;51:5810-31. DOI
3. Tian P, Wei Y, Ye M, Liu Z. Methanol to Olefins (MTO): from fundamentals to commercialization. *ACS Catal* 2015;5:1922-38. DOI
4. Bjorgen M, Svelle S, Joensen F, et al. Conversion of methanol to hydrocarbons over zeolite H-ZSM-5: On the origin of the olefinic species. *J Catal* 2007;249:195-207. DOI
5. Ilias S, Bhan A. Mechanism of the catalytic conversion of methanol to hydrocarbons. *ACS Catal* 2013;3:18-31. DOI
6. Sun X, Mueller S, Liu Y, et al. On reaction pathways in the conversion of methanol to hydrocarbons on HZSM-5. *J Catal* 2014;317:185-97. DOI
7. Yarulina I, Chowdhury AD, Meirer F, Weckhuysen BM, Gascon J. Recent trends and fundamental insights in the methanol-to-hydrocarbons process. *Nat Catal* 2018;1:398-411. DOI
8. Lin S, Zhi Y, Chen W, et al. Molecular routes of dynamic autocatalysis for methanol-to-hydrocarbons reaction. *J Am Chem Soc* 2021;143:12038-52. DOI
9. Erichsen M, Svelle S, Olsbye U. H-SAPO-5 as methanol-to-olefins (MTO) model catalyst: Towards elucidating the effects of acid

strength. *J Catal* 2013;298:94-101. DOI
10. Liu Z, Huang J. Fundamentals of the catalytic conversion of methanol to hydrocarbons. *Chem Synth* 2022;2:21. DOI
11. Zhang L, Liu N, Dai C, et al. Recent advances in shape selectivity of MFI zeolite and its effect on the catalytic performance. *Chem Synth* 2023;3:2. DOI
12. Sullivan RF, Egan CJ, Langlois GE, Sieg RP. A new reaction that occurs in the hydrocracking of certain aromatic hydrocarbons. *J Am Chem Soc* 1961;83:1156-60. DOI
13. Mole T, Bett G, Seddon D. Conversion of methanol to hydrocarbons over ZSM-5 zeolite: An examination of the role of aromatic hydrocarbons using 13carbon- and deuterium-labeled feeds. *J Catal* 1983;84:435-45. DOI
14. Mole T, Whiteside JA, Seddon D. Aromatic co-catalysis of methanol conversion over zeolite catalysts. *J Catal* 1983;82:261-6. DOI
15. Sassi A, Wildman MA, Ahn HJ, Prasad P, Nicholas JB, Haw JF. Methylbenzene chemistry on zeolite HBeta: multiple insights into methanol-to-olefin catalysis. *J Phys Chem B* 2002;106:2294-303. DOI
16. Sassi A, Wildman MA, Haw JF. Reactions of butylbenzene isomers on zeolite HBeta: methanol-to-olefins hydrocarbon pool chemistry and secondary reactions of olefins. *J Phys Chem B* 2002;106:8768-73. DOI
17. Wang S, Chen Y, Wei Z, et al. Polymethylbenzene or alkene cycle? Theoretical study on their contribution to the process of methanol to olefins over H-ZSM-5 zeolite. *J Phys Chem C* 2015;119:28482-98. DOI
18. Ilias S, Bhan A. The mechanism of aromatic dealkylation in methanol-to-hydrocarbons conversion on H-ZSM-5: What are the aromatic precursors to light olefins? *J Catal* 2014;311:6-16. DOI
19. Song W, Fu H, Haw JF. Supramolecular origins of product selectivity for methanol-to-olefin catalysis on HSAPO-34. *J Am Chem Soc* 2001;123:4749-54. DOI PubMed
20. Wang N, Zhi Y, Wei Y, et al. Molecular elucidating of an unusual growth mechanism for polycyclic aromatic hydrocarbons in confined space. *Nat Commun* 2020;11:1079-90. DOI PubMed PMC
21. Haw JF, Song W, Marcus DM, Nicholas JB. The mechanism of methanol to hydrocarbon catalysis. *Acc Chem Res* 2003;36:317-26. DOI PubMed
22. Bjørgen M, Joensen F, Lillerud K, Olsbye U, Svelle S. The mechanisms of ethene and propene formation from methanol over high silica H-ZSM-5 and H-beta. *Catal Today* 2009;142:90-7. DOI
23. Shen Y, Le TT, Fu D, et al. Deconvoluting the competing effects of zeolite framework topology and diffusion path length on methanol to hydrocarbons reaction. *ACS Catal* 2018;8:11042-53. DOI
24. Wang S, Wang P, Qin Z, et al. Relation of catalytic performance to the aluminum siting of acidic zeolites in the conversion of methanol to olefins, viewed via a comparison between ZSM-5 and ZSM-11. *ACS Catal* 2018;8:5485-505. DOI
25. Ding J, Zhang Z, Meng C, Zhao G, Liu Y, Lu Y. From nano- to macro-engineering of ZSM-11 onto thin-felt stainless-steel-fiber: Steam-assisted crystallization synthesis and methanol-to-propylene performance. *Catalysis Today* 2020;347:10-7. DOI
26. Dyballa M, Becker P, Trefz D, et al. Parameters influencing the selectivity to propene in the MTO conversion on 10-ring zeolites: directly synthesized zeolites ZSM-5, ZSM-11, and ZSM-22. *Appl Catal A* 2016;510:233-43. DOI
27. Wang S, Li S, Zhang L, et al. Insight into the effect of incorporation of boron into ZSM-11 on its catalytic performance for conversion of methanol to olefins. *Catal Sci Technol* 2017;7:4766-79. DOI
28. Wang S, Zhang L, Li S, et al. Tuning the siting of aluminum in ZSM-11 zeolite and regulating its catalytic performance in the conversion of methanol to olefins. *J Catal* 2019;377:81-97. DOI
29. Yuan K, Jia X, Wang S, et al. Regulating the distribution of acid sites in ZSM-11 zeolite with different halogen anions to enhance its catalytic performance in the conversion of methanol to olefins. *Microporous Mesoporous Mater* 2022;341:112051. DOI
30. Liu Z, Dong X, Zhu Y, et al. Investigating the influence of mesoporosity in zeolite beta on its catalytic performance for the conversion of methanol to hydrocarbons. *ACS Catal* 2015;5:5837-45. DOI
31. Dai W, Wu G, Li L, Guan N, Hunger M. Mechanisms of the deactivation of SAPO-34 materials with different crystal sizes applied as MTO catalysts. *ACS Catal* 2013;3:588-96. DOI
32. Zhu X, Hofmann JP, Mezari B, et al. Trimodal porous hierarchical SSZ-13 zeolite with improved catalytic performance in the methanol-to-olefins reaction. *ACS Catal* 2016;6:2163-77. DOI
33. Verboekend D, Chabaneix AM, Thomas K, Gilson J, Pérez-ramírez J. Mesoporous ZSM-22 zeolite obtained by desilication: peculiarities associated with crystal morphology and aluminium distribution. *Cryst Eng Comm* 2011;13:3408-16. DOI
34. Selzer C, Biemelt T, Werner A, Kaskel S. Hierarchical zeolite ZSM-58 as shape selective catalyst for methanol-to-olefins reaction. *Microporous Mesoporous Mater* 2018;261:51-7. DOI
35. Madeira F, Ben Tayeb K, Pinard L, Vezin H, Maury S, Cadran N. Ethanol transformation into hydrocarbons on ZSM-5 zeolites: influence of Si/Al ratio on catalytic performances and deactivation rate. Study of the radical species role. *Appl Catal A* 2012;443-444:171-80. DOI
36. Corma A, Fornés V, Forni L, Márquez F, Martínez-triguero J, Moscotti D. 2,6-Di-Tert-Butyl-Pyridine as a probe molecule to measure external acidity of zeolites. *J Catal* 1998;179:451-8. DOI
37. Góra-marek K, Tarach K, Choi M. 2,6-Di- *tert*- butylpyridine sorption approach to quantify the external acidity in hierarchical zeolites. *J Phys Chem C* 2014;118:12266-74. DOI
38. Fan S, Wang H, He S, et al. Formation and evolution of methylcyclohexene in the initial period of methanol to olefins over H-ZSM-5. *ACS Catal* 2022;12:12477-87. DOI
39. Liang T, Chen J, Qin Z, et al. Conversion of methanol to olefins over H-ZSM-5 zeolite: reaction pathway is related to the framework

aluminum siting. *ACS Catal* 2016;6:7311-25. DOI

40. Xue Y, Li J, Wang S, et al. Co-reaction of methanol with butene over a high-silica H-ZSM-5 catalyst. *J Catal* 2018;367:315-25. DOI
41. Price GL, Iglesia E. Matrix method for correction of mass spectra in deuterium-exchange applications. *Ind Eng Chem Res* 1989;28:839-44. DOI
42. Vjunov A, Fulton JL, Huthwelker T, et al. Quantitatively probing the Al distribution in zeolites. *J Am Chem Soc* 2014;136:8296-306. DOI
43. Dedecek J, Lucero MJ, Li C, et al. Complex analysis of the aluminum siting in the framework of silicon-rich zeolites. A case study on ferrierites. *J Phys Chem C* 2011;115:11056-64. DOI
44. Lin LF, Zhao SF, Zhang DW, Fan H, Liu YM, He MY. Acid strength controlled reaction pathways for the catalytic cracking of 1-Pentene to propene over ZSM-5. *ACS Catal* 2015;5:4048-59. DOI
45. Khare R, Millar D, Bhan A. A mechanistic basis for the effects of crystallite size on light olefin selectivity in methanol-to-hydrocarbons conversion on MFI. *J Catal* 2015;321:23-31. DOI
46. Wang C, Wang Q, Xu J, et al. Direct detection of supramolecular reaction centers in the methanol-to-olefins conversion over zeolite H-ZSM-5 by ^{13}C-^{27}Al solid-state NMR spectroscopy. *Angew Chem Int Ed Engl* 2016;55:2507-11. DOI
47. Park JW, Kim SJ, Seo M, Kim SY, Sugi Y, Seo G. Product selectivity and catalytic deactivation of MOR zeolites with different acid site densities in methanol-to-olefin (MTO) reactions. *Appl Catal A* 2008;349:76-85. DOI
48. Wang J, Wei Y, Li J, et al. Direct observation of methylcyclopentenyl cations (MCP^+) and olefin generation in methanol conversion over TON zeolite. *Catal Sci Technol* 2016;6:89-97. DOI
49. Zhang J, Huang Z, Xu L, et al. Verifying the olefin formation mechanism of the methanol-to-hydrocarbons reaction over H-ZSM-48. *Catal Sci Technol* 2019;9:2132-43. DOI